Pressure Facility Effects on the Impedance Characteristics of a 9-kW HET

IEPC-2024-808

Presented at the 38th International Electric Propulsion Conference
Pierre Baudis Convention Center • Toulouse, France
June 23-28, 2024

Janice D. Cabrera[1]
Georgia Institute of Technology, Atlanta, GA, 30318, USA

David R. Jovel[2]
The Aerospace Corporation, El Segundo, California, 90245, USA

Mitchell L. R. Walker[3]
Georgia Institute of Technology, Atlanta, GA, 30318, USA

The effects of increasing the background pressure on the impedance profile of a 9-kW Hall effect thruster from 100 Hz – 300 kHz operated on krypton are examined. The thruster was operated at the 300 V, 15 A and 300 V, 20 A thruster operating conditions. The background pressure varied between 6.8×10^{-6} Torr-Kr and 2×10^{-5} Torr-Kr at the 300 V, 15 A condition, and between 8.5×10^{-6} Torr-Kr and 2.5×10^{-5} Torr-Kr at the 300 V, 20 A condition. At each elevated background pressure, the anode and cathode mass flow rates are varied to maintain a constant discharge current. At the 300 V, 15 A operating condition, the discharge current peak-to-peak values decreased by 6% and 18% as the background pressure was increased by two and three times that of nominal operational pressure. At the same operating condition, the amplitude of the discharge current's power spectral density plot decreased by 44% in the mid-pressure case and 78% in the high-pressure case at the breathing mode frequency. The magnitude of impedance at the breathing mode frequency also displayed a similar trend as it decreased by 29% and 50% as the background pressure increased by two and three times that of the operating pressure. At frequencies above the breathing mode, the magnitude of impedance increased as the pressure increased. At the 300 V, 20 A operating condition, there are no discernable trends observed in the discharge current and cathode-to-ground potential. The amplitude of the discharge current's power spectral density plot decreased by 55% at the mid-pressure case and 90% at the low-pressure case at the breathing mode frequency. The magnitude of impedance did not display a similar trend as the amplitude of the power spectral density plot. Additionally, estimates of the capacitance at the breathing mode show that the capacitance increases as background pressure increases.

Nomenclature

F_{BM}	=	breathing mode frequency, Hz
$\dot{m}_{anode}$	=	anode mass flow rate, mg/s
I_{IC}	=	inner magnet current, A
I_{OC}	=	outer magnet current, A
$I_{dis,mean}$	=	mean discharge current, A

[1] Graduate Research Assistant, School of Aerospace Engineering, jcabrera37@gatech.edu
[2] Engineering Specialist, The Aerospace Corporation, david.r.jovel@aero.org
[3] Chair, School of Aerospace Engineering, mitchell.walker@ae.gatech.edu

$I_{dis,pk2pk}$ = peak-to-peak discharge current, A
$I_{dis,rms}$ = root mean square discharge current, A
PSD = power spectral density
$V_{CG,mean}$ = mean cathode to ground potential, V
$V_{CG,pk2pk}$ = peak-to-peak cathode to ground potential, V
$V_{dis,mean}$ = mean discharge voltage, V
$V_{dis,mean}$ = peak-to-peak discharge voltage, V
Z = impedance magnitude, Ω
θ = impedance phase, °

I.Introduction

The behavior of Hall effect thruster (HET) is influenced by the vacuum test facility and the background environment that results from it. The effects caused by the facility are collectively referred to as facility effects. They are classified into the following categories: contamination, electrical, thermal, and pressure. Evidence of these facility effects on a thruster's stability and performance include elevated erosion rates on thruster hardware due to material sputtering, enhanced ion-electron recombination rates due to free electrons provided by metallic test facilities, elevated background pressures due to the high thermal loading on cryogenic vacuum pumping systems and increased thrust measurements due to neutral ingestion. Understanding the impact of facility effects on thruster behavior in vacuum test facilities will allow us to predict its behavior in the space environment.

Several studies have been conducted over the years to characterize the effect of background pressure on HET performance. Randolph *et al.* established a criterion for acceptable background pressures below 5×10^{-5} Torr to acquire reliable performance data on the SPT-100 [1]. Walker and Gallimore observed increases in discharge current and thrust of a cluster of two 5-kW HETs as the facility background pressure was elevated [2]. Similar results have been achieved on different hall thrusters while maintaining the total mass flow rate constant. Kamhawi *et al.* observed higher discharge current peak-to-peak, discharge current root mean square, and breathing mode frequency from the power spectral density (PSD) analysis of the discharge current waveform with increased facility pressure [3]. The performance and stability of a hall thruster are thus clearly affected by background pressure.

Recently, Jovel developed a novel impedance measurement tool to observe the dynamic behavior of Hall thrusters [4]. The work provides an alternative method to characterize the discharge load of a HET aside from conducting a PSD analysis of the discharge current. It shows that the impedance magnitude and phase profiles of a 7-kW HET from 100 Hz to 300 kHz match well with key characteristics of the PSD of the discharge current such as the breathing mode frequency. Additionally, the resistance and reactance profiles from 100 Hz to 300 Hz are presented for the discharge load. By examining the frequency content in this way, the resistive, capacitive, and inductive behavior within the impedance profile of a HET are quantified. The breathing mode capacitance and inductance are also estimated from the reactance profile. Hence, the impedance profile of a HET provides an additional perspective on the AC characteristics in a HET's frequency domain behavior.

The objective of this paper is to investigate the effects of background pressure on the impedance profile from 100 Hz – 300 kHz of a 9-kW HET operated on krypton. The impedance measurement technique developed by Jovel was used to measure the impedance profiles across three background pressures ranging from 8.5×10^{-6} Torr-Kr to 2.5×10^{-5} Torr-Kr at the following thruster operating conditions: 300 V, 15 A and 300 V, 20 A.[4] In order to determine the effect of background pressure on the impedance characteristics of the HET, the changes in impedance magnitude and phase are quantified. The resistance and reactance profiles are extracted to further characterize the changes observed in the impedance characteristics of the thruster as a result of increased background pressure. These trends are compared to those observed in the time-resolved discharge current, discharge voltage, and cathode-to-ground potential waveform traces to further support the results from the impedance measurements.

The paper is organized as follows. Section II provides an overview of how impedance spectroscopy is applied to the discharge load of a HET. In Section III, the experimental setup is provided including the vacuum test facility, thruster, and diagnostics used. In Section IV, the impedance profiles of a 9-kW hall thruster at the 300 V, 15 A, and 300 V, 20 A operating conditions are shown. In Section V, the results from the PSD of the discharge current are compared to the impedance profiles at each background pressure. Furthermore, the resistance and reactance profiles are obtained to quantify the effect of the background pressure on the dynamic behavior of a HET in relation to resistive, inductive, and capacitive behavior changes. In Section VI, the conclusions from conducting this pressure facility effects work are presented.

The 38th International Electric Propulsion Conference, P. Baudis Convention Center, Toulouse, France June 23-28, 2024

II.Overview of Impedance Spectroscopy

Impedance is the summation of the real resistance and imaginary reactance of an electrical load. The magnitude of impedance is calculated by dividing the magnitude of voltage by the magnitude of current for a given circuit at a frequency. The phase of impedance is the phase angle difference between the voltage and current at a given frequency. Therefore, an electrical load's impedance is defined by its magnitude and phase at a specific frequency.

Impedance spectroscopy is an electrical engineering technique used to measure a load's impedance in the frequency domain. It measures the impedance given the current response resulting from an applied, known voltage signal. However, this technique assumes the electrical load behaves as a linear, time-invariant system. A linear system is one that adheres to homogeneity, requiring the transfer function between the input and output signals to scale proportionally. A load is considered time-invariant if the transfer function of the input and output signals are constant in time. Before the impedance of an electrical load can be determined using impedance spectroscopy, the load's behavior must be shown to be linear and time-invariant.

The discharge of a HET can be viewed as a complex electrical load that is governed by plasma conductivity, which is affected by the charged and neutral particle densities that vary in time and space. Because of the various processes that occur throughout the entire plasma environment, the discharge load is defined as dynamic, with a DC discharge current and a time-varying AC discharge component. Jovel showed that the HET electrical load is nonlinear and time-variant.[4] However, they provided alternative techniques within electrical engineering that can be used on nonlinear and time-variant loads that are applicable within a localized region around its DC component.

Small signal impedance analysis is an effective technique for estimating the impedance of nonlinear electrical loads by adding a small perturbation around their DC operating point. The perturbation must be greater than the signal's noise content but small enough that its effect linearizes around the DC operating condition. The impedance of the discharge load is measured in this work using the same 2-V peak amplitude voltage signal as in previous works.

III.Experimental Setup

In this section, the thruster, vacuum test facility, and diagnostics involved with the experiment are discussed.

A. Test Article

The H9 HET serves as the HET testbed in this experiment. It was developed by the University of Michigan, the Air Force Research Laboratory, and the Jet Propulsion Laboratory [5]. The H9 uses a center-mounted lanthanum hexaboride hollow cathode. Figure 1 shows an image of the thruster operating in the test facility. For this experiment, the thruster is operated in a grounded-body electrical configuration on krypton at the thruster operating conditions listed in Table 1. The cathode flow fraction is 7%.

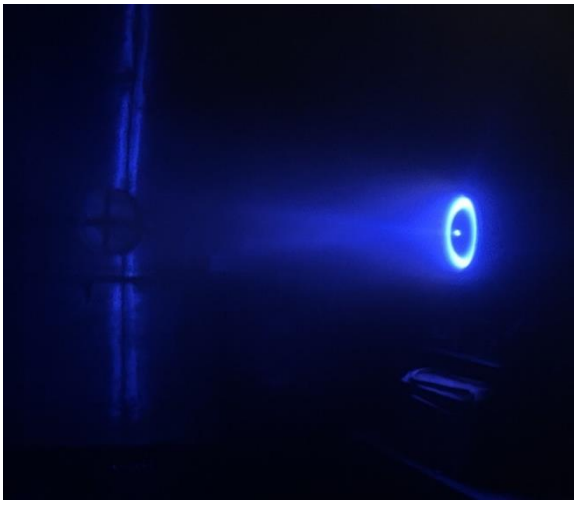

Figure 1. The H9 HET operating on krypton

Table 1. H9 operating conditions on krypton

V_{dis} [V]	I_{dis} [A]	$\dot{m}_{anode}$ [mg/s]	I_{IC} [A]	I_{OC} [A]
300	15	11.37	4.7	2.6
300	20	14.33	4.11	2.28

A 50-kW DC power supply manufactured by Magna-Power sustains the thruster discharge. To protect the discharge power supply, an RC filter consisting of a 0.53-Ω resistor and a 100-μF capacitor is placed in between the power supply and thruster discharge power lines. A Teledyne LeCroy HDO6104 oscilloscope measures time-resolved discharge current, discharge voltage, and cathode-to-ground potential measurements. A Teledyne Lecroy CP150 current probe is used to measure the discharge current. The current probe is placed on the low side of the discharge circuit, upstream of the RC discharge filter. The discharge voltage is measured using a Powertek DP25 high-voltage differential probe placed at the chamber power feedthrough. The discharge current, discharge voltage, and cathode-to-ground potential measurements are recorded on individual channels at a sampling frequency of 10 Ms/s. Additionally, two MKS GE50A mass flow meters are used to set the mass flow rates of the anode and the cathode.

B. Vacuum Test Facility

Experiments are conducted at the Georgia Institute of Technology's High-Power Electric Propulsion Laboratory in Vacuum Test Facility 2. The stainless-steel chamber measures 4.9 m in diameter by 9.2 m in length. Low base pressures of 2 × 10-8 Torr-N_2 are achieved via 10 liquid nitrogen cooled PHPK TMI1200i cryopumps that provide a nominal pumping speed of 350 kl/s on xenon. The facility features a closed-loop, liquid nitrogen liquefaction system.

A Varian 571 ion gauge Bayard-Alpert hot filament ion gauge measures the facility pressure 1 m away from the thruster exit plane. A neutralizer is installed on the gauge to reduce ion collection [6]. The pressure measurements are displayed by an Agilent XGS-600 controller and recorded using LabView software.

The background pressure is increased by bleeding in krypton using a ¼" Swagelok tube fitting placed 1.8 m downstream of the HET exit plane and 1 m below the HET. The bleed line is aligned with the thruster centerline with the orifice directed towards the chamber wall. A MKS GE50A mass flow meter is used to bleed in sufficient krypton to elevate the background pressure to the desired value. For the 300 V, 15 A thruster operating condition, a nominal operational pressure of 6.8×10^{-6} Torr-Kr is achieved. Krypton is bled in to elevate the background pressure to 1.3×10^{-5} Torr- Kr and 2×10^{-5} Torr-Kr such that the background pressure is double and triple that of the nominal operational pressure. For the 300 V, 20 A thruster operating condition, a nominal operational pressure of 8.5×10^{-6} Torr-Kr is recorded. Similarly, krypton is bled in to elevate the background pressure to 1.6×10^{-5} Torr- Kr and 2.5×10^{-5} Torr-Kr to double and triple the nominal operational pressure. At each elevated background pressure, the anode and cathode mass flow rates are adjusted to maintain a constant discharge current. Typically, the mass flow rate to the thruster must be reduced as the chamber operating pressure increases to maintain a constant discharge current.

C. Impedance Measurement Diagnostic

Figure 2 shows an electrical schematic of the impedance measurement diagnostic setup. The Powertek GP1700 Analyzer serves as a frequency response analyzer to provide the excitation signal to the discharge load as well as record the current and voltage response due to the excitation signal. The AE Techron 7234 power amplifier amplifies the excitation signal provided by the GP1700 as well as enables current flow in the coupling circuit. Additionally, the AE Techron T2000 isolation transformer couples to the discharge circuit and injects the excitation signal by the GP1700 into the discharge current. The current response due to the excitation signal is measured by a Pearson 804 current meter located less than 0.5 m away from the chamber power feedthrough. Similarly, the voltage response is measured at the same location away from the chamber with a Powertek DP25 high-voltage differential probe. Moreover, the calibration procedure developed by Jovel was used to remove the impedance from all harnessing and electrical connections from the discharge power supply to the thrust stand [4].

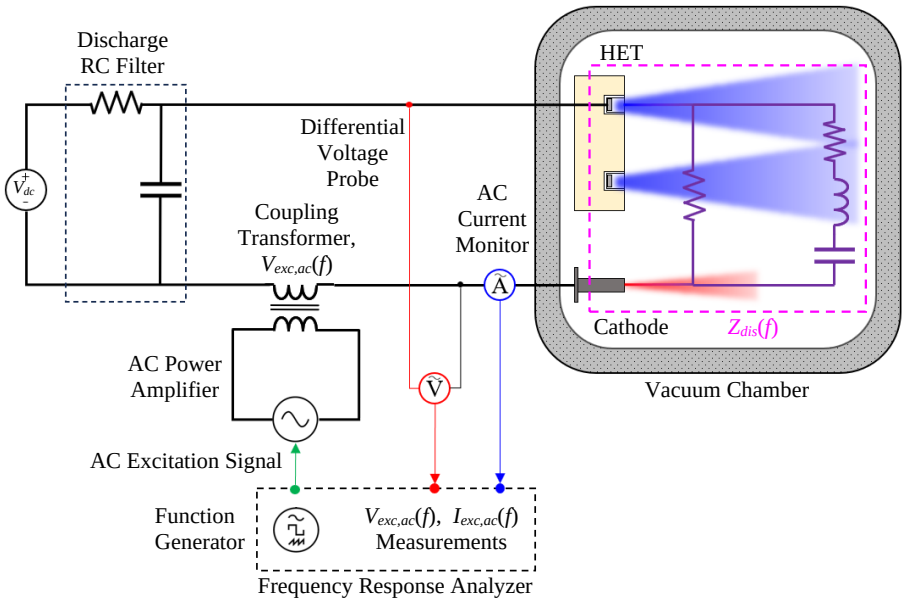

Figure 2. Impedance measurement setup *[4]*

IV.Results

In this section, the average impedance magnitude and phase diagrams from 100 Hz to 300 kHz are displayed. First, the impedance profiles at the 6.8 × 10^{-6} Torr-Kr, 1.3 × 10^{-5} Torr-Kr, and 2.0 × 10^{-5} Torr-Kr background pressures at the 300 V, 15 A operating condition are presented. Next, the impedance profiles at the 6.8 × 10^{-6} Torr-Kr, 1.3 × 10^{-5} Torr-Kr, and 2.0 × 10^{-5} Torr-Kr background pressures at the 300 V, 20 A operating conditions are presented.

A. Background Pressure Effect on Impedance Magnitude and Phase at 300 V , 15 A Operating Condition

Figures 3 and 4 show the impedance magnitude and phase at the 300 V and 15 A thruster operating condition, respectively, from 100 Hz to 300 kHz at each of the three pressures. The blue line is the low background pressure, the red line is the mid background pressure, and the yellow line is the high background pressure case. The magnitude is nearly constant across the three pressures at about 1.7 Ω from 100 Hz to 2 kHz before it rapidly rises to approximately 4 kHz. The low-operational pressure impedance profile has a sharp peak at 15.08 kHz with a magnitude of 9.3 Ω followed by a drop in phase from 42.9˚ to -25.1˚. The mid-operational pressure impedance profile has a sharp peak at 14.60 kHz with a magnitude of 6.5 Ω followed by a drop in phase from 39.8˚ to -8.2˚. The high operational pressure impedance profile has a sharp peak at 14.98 kHz with a magnitude of 4.6 Ω followed by a drop in phase from 35.6˚ to 8.8˚.

The magnitude of the impedance across the three pressures continues to increase until another peak is observed. The second peak occurs at 135.02 kHz with a magnitude of 13.6 Ω in the low-pressure case. The second peak for the mid-pressure case occurs at 134.1 kHz with a magnitude of 14.1 Ω. For the high-pressure case, the second peak occurs at 131.58 kHz with a magnitude of 14.6 Ω.

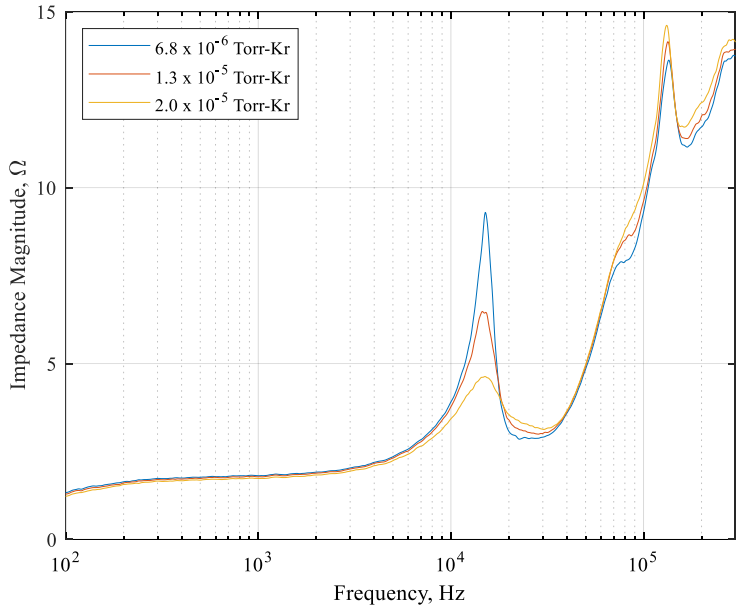

Figure 3. Impedance magnitude as a function of frequency at the 300 V, 15 A thruster operating condition

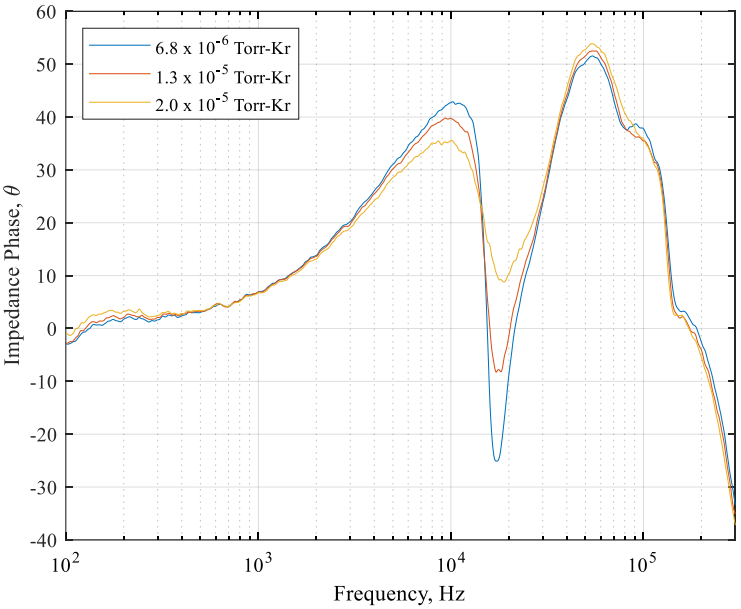

Figure 4. Impedance phase as a function of frequency at the 300 V, 15 A thruster operating condition

B. Background Pressure Effect on Impedance Magnitude and Phase at 300 V, 20 A Operating Condition

Figures 5 and 6 show the impedance magnitude and phase at the 300 V and 20 A thruster operating condition, respectively, from 100 Hz to 300 kHz at each of the three pressures. Similarly, the blue line is the low background pressure, the red line is the mid background pressure, and the yellow line is the high background pressure case. The magnitude is nearly constant across the three pressures at about 2 Ω from 100 Hz to 1 kHz before it quickly increases to approximately 3 kHz. The low-operational pressure impedance profile has a dominant peak at 13.42 kHz with a magnitude of 11.8 Ω followed by a drop in phase from 31.2˚ to -83.3˚. The mid-operational pressure impedance profile

has a dominant peak at 13.00 kHz with a magnitude of 9.0 Ω followed by a drop in phase from 29.2˚ to -80.6˚. The high operational pressure impedance profile has a dominant peak at 12.20 kHz with a magnitude of 9.7 Ω followed by a drop in phase from 31.0˚ to -71.8˚.

The magnitude of impedance increases across the three pressure cases until it reaches a local maximum. The second peak occurs at 28.92 kHz with a magnitude of 4.3 Ω in the low-pressure case along with a decrease in phase from 28.0˚ to -1.4˚. For the mid-pressure case, the second peak occurs at 28.2 kHz with a magnitude of 4.1 Ω along with a decrease in phase from 26.2˚ to 1.8˚. The high-pressure case has a second peak at 28.2 kHz with a magnitude of 3.5 Ω along with a decrease in phase from 27.8˚ to 12.9˚. Past these second peaks, the magnitude of impedance increases with indistinguishable humps across all pressure conditions through 100 kHz. A third discernable peak in the low-pressure case occurs at 144.94 kHz with a magnitude of 8.5 Ω. The third peak occurs at 144.0 kHz with a magnitude of 8.8 Ω in the mid-pressure case. In the high-pressure case, the third peak occurs at 136.77 kHz with a magnitude of 9.2 Ω.

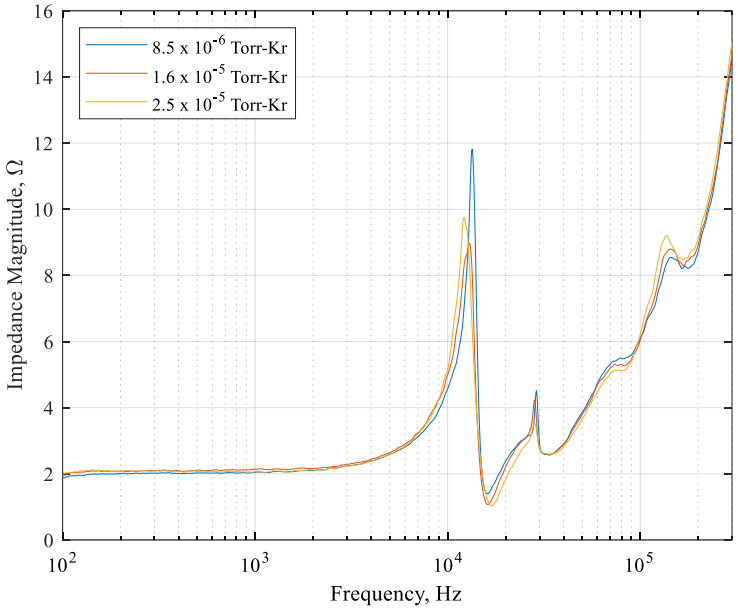

Figure 5. Impedance magnitude as a function of frequency at the 300 V, 20 A thruster operating condition

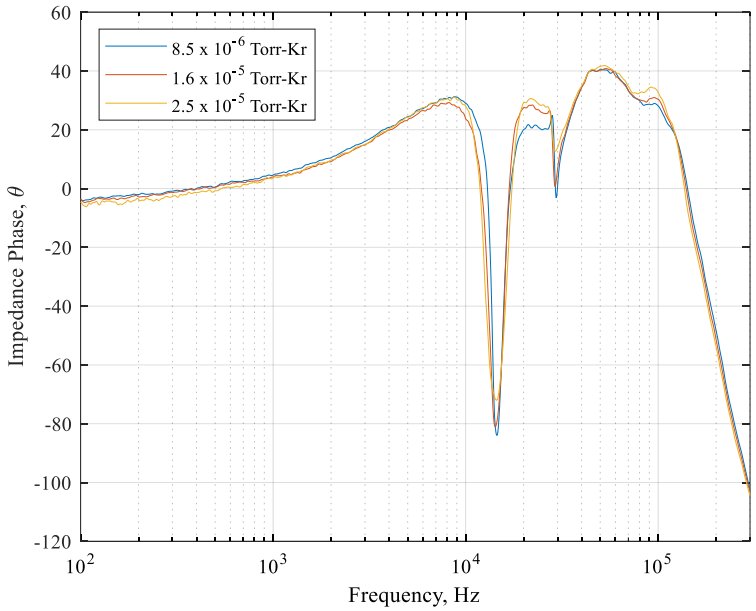

Figure 6. Impedance phase as a function of frequency at the 300 V, 20 A thruster operating condition

V.Discussion

In this section, the impedance profiles across the two operating conditions are analyzed to characterize the effect of background pressure on an electrically grounded thruster inside a vacuum test facility. First, the power spectral density, PSD, of the discharge current at the various background pressures are compared between each other. These findings are then compared to those observed in the impedance profiles to support the background pressure effect on the hall thruster discharge load at the two thruster operating conditions. Next, the resistance and reactance across the 100 Hz – 300 kHz frequency range are extracted from the impedance magnitude and phase profiles to correlate the changes observed in the resistive, capacitive, and inductive behavior of the discharge load to changes in background pressure.

A. Background Pressure Effect on PSD of I_{dis} and Impedance Profile at 300 V, 15 A Operating Condition

Figure 7 shows the PSD of the discharge current, I_{dis}, which is representative of the energy distribution of the discharge current signal across the frequency range of 100 Hz – 300kHz at the 300 V, 15 A operating condition. The blue line is the low background pressure, the red line is the mid-background pressure, and the yellow line is the high background pressure. The frequency with the greatest energy content is assumed to be the breathing mode frequency, F_{BM}. Given the noise present in the signal, a gaussian fit is used to estimate the breathing mode frequency. The uncertainty of the F_{BM} is provided by the full-width, half-maximum range. Along with this parameter, the mean discharge current, $I_{dis,mean}$, and peak-to-peak discharge current, $I_{dis,pk2pk}$, for the same waveform trace are extracted at each pressure condition, listed in Table 1. The mean discharge current across the three pressure cases is held at 15 A by varying the total mass flow rate while maintaining a 7% cathode flow fraction. The $I_{dis,pk2pk}$ is reduced by nearly 6% at a background pressure twice that of the operational pressure and 18% at a background pressure three times that of the operational pressure. The presence of additional neutrals in the plasma environment at this operating condition dampens the breathing mode amplitude as well as seen in the PSD plot. The amplitude decreased by about 44% in the mid-pressure condition and about 78% in the high-pressure condition with respect to the low-pressure condition. The F_{BM} also shifted to the right as the background pressure increased, but they are all within 2 kHz of each other.

Moreover, the cathode-to-ground potential, V_{CG}, decreases as the background pressure increases. Similar to the trend observed in $I_{dis,pk2pk}$, the peak-to-peak cathode to ground potential, $V_{CG,pk2pk}$, also decreased as pressure increased.

The 38th International Electric Propulsion Conference, P. Baudis Convention Center, Toulouse, France June 23-28, 2024

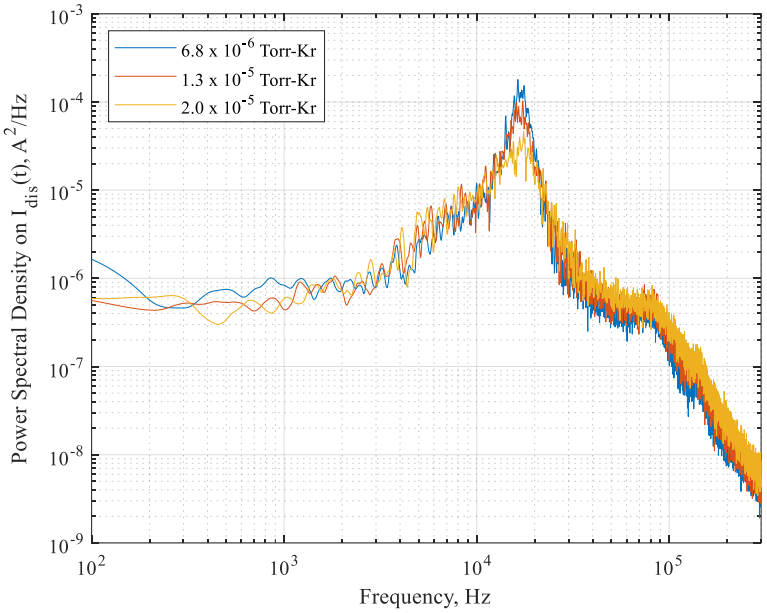

Figure 7. PSD of I_{dis} as a function of frequency at the 300 V, 15 A thruster operating condition

Table 2. Time-averaged discharge characteristics at the 300 V, 15 A thruster operating condition

Pressure [Torr-Kr]	$I_{dis,\,mean}$ [A]	$I_{dis,\,pk2pk}$ [A]	$V_{dis,\,mean}$ [V]	$V_{dis,\,pk2pk}$ [V]	V_{CG} [V]	$V_{CG,\,pk2pk}$ [V]	F_{BM} [kHz]
6.8×10^{-6}	15.03	4.46	299.93	50.37	-17.52	17.21	16.37 ± 1.54
1.5×10^{-5}	15.03	4.19	299.93	50.41	-17.94	16.47	16.11 ± 1.70
2.0×10^{-5}	15.00	3.68	300.11	49.42	-18.49	15.43	17.83 ± 2.55

The impedance magnitude and phase in Figures 3 and 4 also display similar trends. As shown by Jovel, the dominant peak in the impedance magnitude plot can be correlated to the F_{BM} determined from the PSD of the I_{dis}. Therefore, the differences in the impedance profiles at the F_{BM} can be analyzed across the background pressures as done in the PSD plot. The magnitude of impedance decreased by 29% at the mid-pressure case with a phase difference of 30% in comparison to the low-pressure case. For the high-pressure case, the magnitude of impedance decreased by 50% along with a phase difference of 61%. Although the F_{BM} shifted to the left, it remained within 0.5 kHz between each other.

B. Background Pressure Effect on PSD of I_{dis} and Impedance Profile at 300 V, 20 A Operating Condition

Likewise, a similar analysis is performed at the 300 V, 20 A thruster operating condition. Figure 8 shows the PSD of the I_{dis}. Table 2 presents the discharge current, discharge voltage, and cathode-to-ground potential characteristics. The $I_{dis,pk2pk}$ increased slightly by 1% at double the nominal operational pressure and decreased by 5% at triple the nominal operational pressure. The PSD's amplitude at the F_{BM} decreased by approximately 55% at the mid-pressure condition while the amplitude decreased by about 90% at the high-pressure condition. There is not a discernible difference between the F_{BM} itself across the pressure cases as they stayed within 0.5 kHz of each other.

Furthermore, the cathode-to-ground potential, V_{CG}, decreases as the background pressure increases. However, the $V_{CG,pk2pk}$ does not present a noticeable trend as in the $I_{dis,pk2pk}$.

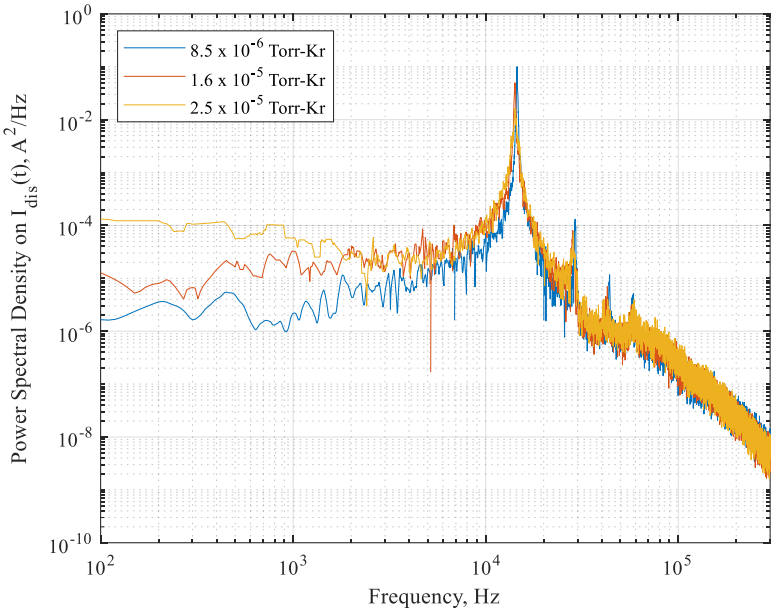

Figure 8. PSD of I_{dis} as a function of frequency at the 300 V, 20 A thruster operating condition

Table 3. Time-averaged discharge characteristics at the 300 V, 20 A thruster operating condition

Pressure [Torr-Kr]	$I_{dis,\ mean}$ [A]	$I_{dis,\ pk2pk}$ [A]	$V_{dis,\ mean}$ [V]	$V_{dis,\ pk2pk}$ [V]	V_{CG} [V]	$V_{CG,\ pk2pk}$ [V]	F_{BM} [kHz]
8.2×10^{-6}	20.00	17.42	299.91	75.60	-16.51	35.08	14.54 ± 0.09
1.6×10^{-5}	20.09	17.64	299.96	73.33	-16.89	36.33	14.18 ± 0.15
2.5×10^{-5}	20.13	16.62	299.98	72.50	-17.30	35.54	14.22 ± 0.46

Additionally, the impedance profile at the 300 V, 20 A thruster operating condition is analyzed. The magnitude of impedance decreased by 23% in the mid-pressure case, with a phase difference of 3%, compared to the low-pressure case. For the high-pressure case, the magnitude of impedance decreased by 16% along with a phase difference of 9%. The F_{BM} shifted to the left as the background pressure increased, but they were all within 2 kHz of each other.

C. Background Pressure Effect on Resistance and Reactance at 300 V, 15 A Operating Condition

The resistive, inductive, and capacitive features of an impedance profile can be analyzed from the real and imaginary components of impedance. Figure 9 shows the resistance, the real part of impedance, for the 300 V, 15 A thruster operating condition. Figure 10 shows the reactance, the imaginary part of impedance, for the 300 V, 15 A thruster operating condition. The blue line is the low background pressure condition, the red line is the mid-background pressure condition, and the yellow line is the high background pressure condition. From 100 Hz to 4 kHz, the resistance across the three background pressures is approximately 1.7 Ω. The reactance plot indicates a shift from capacitive to inductive behavior at approximately 800 Hz at each pressure condition. The reactance from 800 Hz to 4 kHz is dominated by inductance with a mean reactance of 0.4 Ω. The resistance quickly begins to rise from 4 kHz to the breathing mode frequencies identified in Section IV at each background pressure. At the low-pressure condition, the F_{BM} of 15.08 kHz has a resistance of 9.3 Ω with a reactance of 0 Ω. At the mid-pressure condition, the F_{BM} of 14.60 kHz has a resistance of 6.5 Ω with a reactance of 0 Ω. At the high-pressure condition, the F_{BM} of 14.98 kHz has a resistance of 6.5 Ω with a reactance of 1.3 Ω. Since a reactance of 0 Ω indicates a resonant frequency, F_{BM} at the low and mid-pressure case is also a resonant frequency. However, the F_{BM} at the high-pressure case is not a resonant frequency.

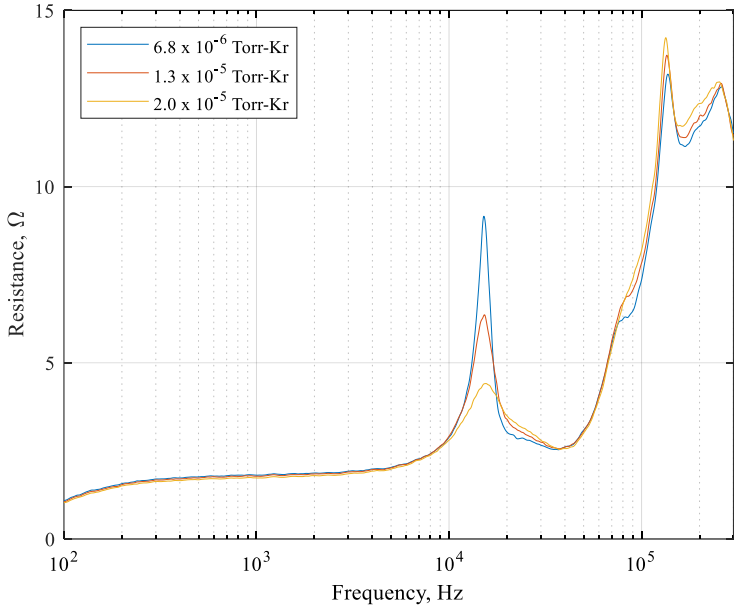

Figure 9. Resistance as a function of frequency at the 300 V, 15 A thruster operating condition

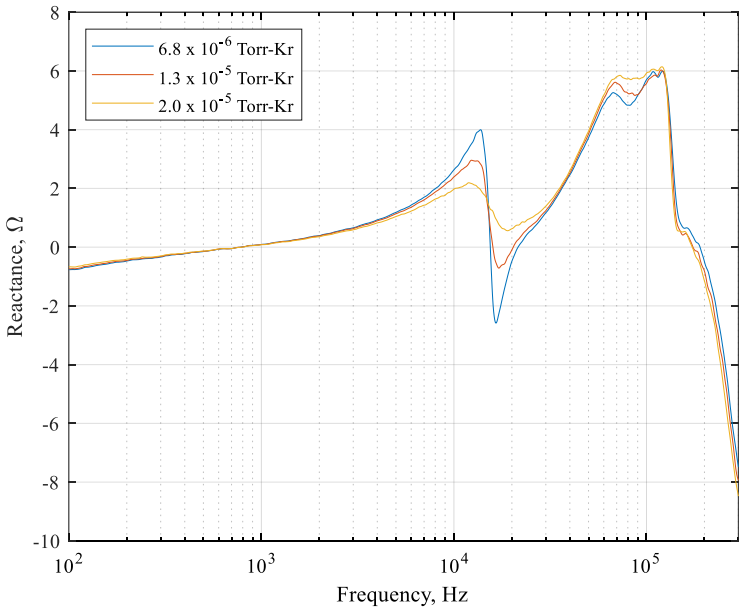

Figure 10. Reactance as a function of frequency at the 300 V, 15 A thruster operating condition

Following the procedure by Jovel, the capacitance at the F_{BM} can be estimated by assuming a purely capacitive and inductive reactance near the F_{BM}. In the low-pressure case, the reactance at $\min\left(\frac{\partial X}{\partial f}\right)$ is –0.10 Ω at 15.47 kHz which yields a breathing mode capacitance of 98.23 μF. At the mid-pressure condition, the reactance at $\min\left(\frac{\partial X}{\partial f}\right)$ is –0.05 Ω at 15.98 kHz which yields a breathing mode capacitance of 199.20 μF.

D. Background Pressure Effect on Resistance and Reactance at 300 V, 20 A Operating Condition

Figure 11 shows the resistance and Figure 12 shows the reactance for the 300 V, 20 A thruster operating condition. From 100 Hz to 4 kHz, the resistance across the three background pressures is approximately 2 Ω. The reactance plot indicates a shift from capacitive to inductive behavior at approximately 1 kHz at each pressure condition. The

reactance from 1 kHz to 4 kHz is dominated by inductance with a mean reactance of 0.4 Ω. The resistance quickly begins to rise from 4 kHz to the breathing mode frequencies identified in Section IV at each background pressure. At the low-pressure condition, the F_{BM} of 13.42 kHz has a resistance of 11.0 Ω with a reactance of 0 Ω. At the mid-pressure condition, the F_{BM} of 13.00 kHz has a resistance of 8.4 Ω with a reactance of 0 Ω. At the high-pressure condition, the F_{BM} of 12.20 kHz has a resistance of 9.6 Ω with a reactance of 0 Ω. All background pressures indicate that the F_{BM} is a resonant frequency.

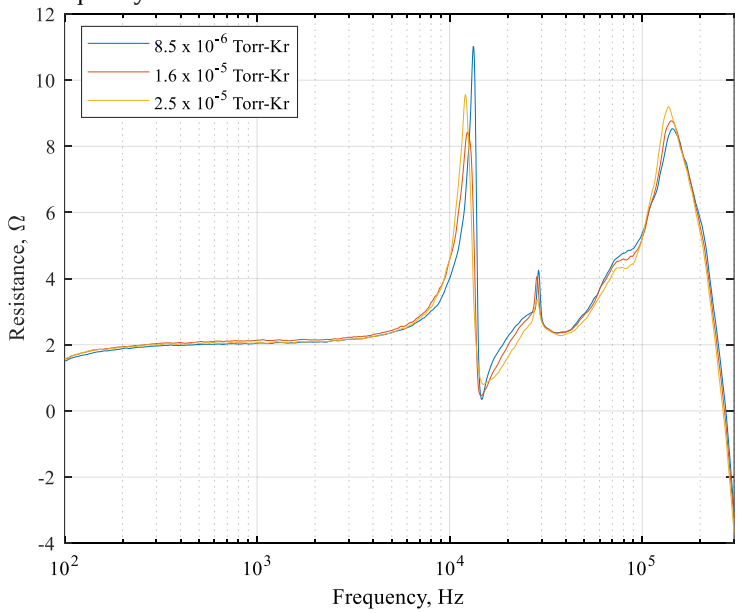

Figure 11. Resistance as a function of frequency at the 300 V, 20 A thruster operating condition

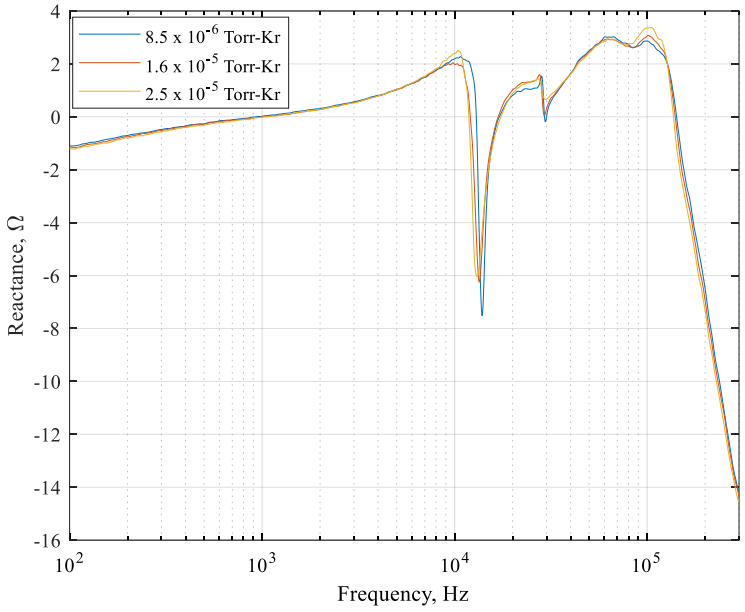

Figure 12. Reactance as a function of frequency at the 300 V, 20 A thruster operating condition

A similar analysis is performed at the second prominent peak identified in Section IV. At the low-pressure condition, the second peak occurs at 28.92 kHz with a resistance of 4.3 Ω with a reactance of 0 Ω. At the mid-pressure condition, the second peak identified at 28.20 kHz has a resistance of 4.1 Ω with a reactance of 0.1 Ω. At the high-

pressure condition, the second peak occurs at 28.20 kHz with a resistance of 3.4 Ω with a reactance of 0.7 Ω. Therefore, only the low-pressure condition yields a second resonant frequency.

Moreover, at the low-pressure case the reactance at $\min\left(\frac{\partial X}{\partial f}\right)$ is –5.38 Ω at 13.51 kHz which yields a breathing mode capacitance of 2.19 μF. At the mid-pressure condition, the reactance at $\min\left(\frac{\partial X}{\partial f}\right)$ is –5.20 Ω at 13.09 kHz which yields a breathing mode capacitance of 2.34 μF. At the high-pressure condition, the reactance at $\min\left(\frac{\partial X}{\partial f}\right)$ is –3.17 Ω at 12.35 kHz which yields a breathing mode capacitance of 4.06 μF.

VI.Conclusion

The impedance of a hall thruster's discharge load is significantly impacted by the background pressure. At the 300 V, 15 A thruster operating condition, the magnitude of impedance at the F_{BM} decreased as the pressure increased. In particular, a background pressure of three times that of the nominal operational pressure resulted in a decrease of 50%. This trend is also identified in the PSD of the I_{dis} at the F_{BM} as well as the peak-to-peak values of I_{dis} and V_{CG}. At the 300 V, 20 A thruster operating condition, the magnitude of impedance at the F_{BM} also generally decreased as the pressure increased. However, the decrease is only observed in the amplitude of the PSD of the I_{dis} at the F_{BM}. Additionally, estimates of the capacitance at the F_{BM} across the thruster operating conditions show that the capacitance increases as the background pressure increases.

Acknowledgments

The work was funded by the Joint Advanced Propulsion Institute, a NASA Space Technology Research Institute, Grant Number 80NSSC21K1118.

References

[1] Randolph, T., Kim, V., Kaufman, H., Kozubsky, K., Zhurin, V. and Day, M., "Facility Effects on Stationary Plasma Thruster Testing," IEPC 93-93, September 1993.

[2] Walker, M.L.R. and Gallimore, A.D., "Performance Characteristics of a Cluster of 5-kW Laboratory Hall Thrusters," Journal of Propulsion and Power, Vol. 23, No. 1, January-February 2007, pp. 35-43.

[3] Kamhawi, H., Huang, W., Haag, T., Yim, J., Herman, D., Peterson, P.Y., Williams, G., Gilland, J., Hofer, R. and Mikellides, I., "Performance, Facility Pressure Effects, and Stability Characterization Tests of NASA's 12.5-kW Hall Effect Rocket with Magnetic Shielding Thruster, " AIAA 2016-4826, July, 2024.

[4] D Jovel, D.R., "Impedance Characterization of a Hall Effect Thruster Discharge in a Ground-based Vacuum Test Facility," Ph.D. Dissertation, Aerospace Engineering Dept., Georgia Institute of Technology, Atlanta, GA, 2024.

[5] R Hofer R.R., Cusson, S.E., Lobbia, R.B. and Gallimore, A.D., "The H9 Magnetically Shielded Hall Thruster," IEPC-2017-232, October 2017.

[6] Dankanich J.W., Walker, M.L.R., Swiatek, M.W. and Yim, J.T., "Recommended Practice for Pressure Measurement and Calculation of Effective Pumping Speed in Electric Propulsion Testing," Journal of Propulsion and Power, Vol. 33, No. 3, May-June 2017, pp. 668-680.